AD_____

Award Number: W81XWH-13-1-0050

TITLE: Development of Ultrasound to Measure In-vivo Dynamic Cervical Spine Intervertebral Disc Mechanics

PRINCIPAL INVESTIGATOR: Brian Snyder

CONTRACTING ORGANIZATION: Beth Israel Deaconess Medical Center.
Boston ,Massachusetts 02215

REPORT DATE: January 2014

TYPE OF REPORT: Annual

PREPARED FOR: U.S. Army Medical Research and Materiel Command
Fort Detrick, Maryland 21702-5012

DISTRIBUTION STATEMENT: Approved for Public Release;
Distribution Unlimited

The views, opinions and/or findings contained in this report are those of the author(s) and should not be construed as an official Department of the Army position, policy or decision unless so designated by other documentation.

REPORT DOCUMENTATION PAGE

Form Approved
OMB No. 0704-0188

Public reporting burden for this collection of information is estimated to average 1 hour per response, including the time for reviewing instructions, searching existing data sources, gathering and maintaining the data needed, and completing and reviewing this collection of information. Send comments regarding this burden estimate or any other aspect of this collection of information, including suggestions for reducing this burden to Department of Defense, Washington Headquarters Services, Directorate for Information Operations and Reports (0704-0188), 1215 Jefferson Davis Highway, Suite 1204, Arlington, VA 22202-4302. Respondents should be aware that notwithstanding any other provision of law, no person shall be subject to any penalty for failing to comply with a collection of information if it does not display a currently valid OMB control number. **PLEASE DO NOT RETURN YOUR FORM TO THE ABOVE ADDRESS.**

1. REPORT DATE	2. REPORT TYPE	3. DATES COVERED
January 2014	Annual	26December2012-26December2013

4. TITLE AND SUBTITLE

Development of Ultrasound to Measure In-vivo Dynamic Cervical Spine Intervertebral Disc Mechanics

5a. CONTRACT NUMBER

5b. GRANT NUMBER
W81XWH-13-1-0050

5c. PROGRAM ELEMENT NUMBER

6. AUTHOR(S)

Brian Snyder, MD

E-Mail: Brian.Snyder@childrens.harvard.edu

5d. PROJECT NUMBER

5e. TASK NUMBER

5f. WORK UNIT NUMBER

7. PERFORMING ORGANIZATION NAME(S) AND ADDRESS(ES)

Beth Israel Deaconess Medical Center
330 Brookline Avenue, Boston, MA 02215

Medical College of Wisconsin
8701 W Watertown Plank Rd, Milwaukee, WI 53226

8. PERFORMING ORGANIZATION REPORT

9. SPONSORING / MONITORING AGENCY NAME(S) AND ADDRESS(ES)

U.S. Army Medical Research and Materiel Command
Fort Detrick, Maryland 21702-5012

10. SPONSOR/MONITOR'S ACRONYM(S)

11. SPONSOR/MONITOR'S REPORT NUMBER(S)

12. DISTRIBUTION / AVAILABILITY STATEMENT
Approved for Public Release; Distribution Unlimited

13. SUPPLEMENTARY NOTES

14. ABSTRACT
We developed a unique dual ultrasound system that can non-invasively measure IVD deformation and mechanical compliance ex-vivo, and provide real-time images of IVDs and dynamic vertebral motion in-vivo during simulated tasks relevant to acute and chronic cervical spine injury and disease. A semi-automated program was developed to track the motion of a user-specified region of interest that corresponds to the anterior and posterior bony profiles of cervical vertebrae. Dynamic IVD displacements of vertebrae C4-5 measured by US were consistent with direct measurements. For motion frequencies up to 8Hz, US accounted for 77-96% of the true IVD displacements. We developed a transfer function that modeled the non-linear displacement of human cadaveric cervical spine functional spine units (FSU) as a function of an applied sinusoidal load that accounts for differential compliance and damping coefficients in tension and compression. A FEM of the cervical spine was updated to be more relevant to the military population. It has improved geometry, uses a finer mesh, has an increased number of elements and includes an additional spine segment. These refinements will improve the capability of the FEM to simulate different types of loadings and expand the model's responsiveness making it more suitable to carry out parametric studies. We developed a diagnostic system that applies dynamic cyclic loads to cervical spine over a range of programmable frequencies and amplitudes that simulate operational conditions.

15. SUBJECT TERMS None provided

16. SECURITY CLASSIFICATION OF:			17. LIMITATION OF ABSTRACT	18. NUMBER OF PAGES	19a. NAME OF RESPONSIBLE PERSON
a. REPORT	b. ABSTRACT	c. THIS PAGE			USAMRMC
U	U	U	UU	20	19b. TELEPHONE NUMBER *(include area code)*

Table of Contents

Introduction:

A dual ultrasound(US) imaging system comprised of two Terason t3200 machines with hardware/software integration was developed to measure 3D motion of contiguous cervical vertebrae and intervertebral discs (IVD) strain (Δheight of IVD/original IVD height) of intervening functional spine units (FSU). This system was validated ex-vivo using cadaveric C-spines mounted in a servo-hydraulic material testing machine by comparing dynamic US measurement to concurrent measurements made directly using a linear variable differential transformer (LVDT) system. After validation, we derived biomechanics model to examine how dynamic forces applied to the occipital-atlanto junction (i.e. base of skull - C1 interface) are transferred to the subaxial C-spine (i.e. cervical spine segments including and caudal to C2) using US to measure the motion of the cervical vertebrae and the deformation of the intervening intervertebral discs (IVD). Additionally, the relationship between the "health" and integrity of IVD assessed from MRI images using the Pfirrmann grade was compared to the "static" compliance of the cadaveric C-spine FSU's calculated by measuring the IVD strain in response to sequentially increasing compressive and distractive forces applied to C1.

Progress on specific task aims proposed in the statement of work:

<u>Task 1</u> Develop dual Ultrasound system capable of measuring motion of cervical vertebrae in response to known static and dynamic loads applied to human C-spine ex-vivo and in-vivo: We collaborated with the commercial US system manufacturer Terason (Burlington, MA) to develop the hardware and software for this unique dual ultrasound system (Figure 1).

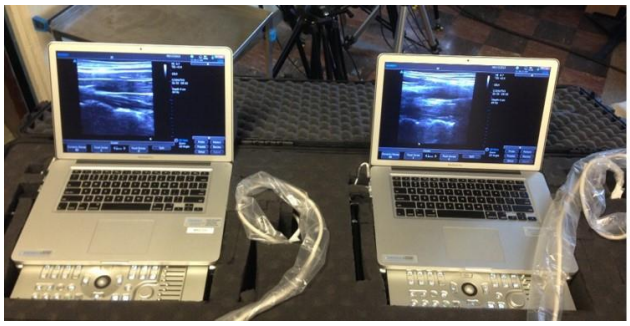

Figure 1. *Dual ultrasound system allows simultaneous imaging of the anterior and posterior C-spine*

<u>Hardware development</u>: A block diagram of the dual ultrasound system's hardware configuration is shown in Figure 2. One of the dual T3200 US devices functions as the master to synchronize signal and data acquisition from the slave device. A "synchronous acquisition" mode was developed by Terason to accomplish this: the master US system sends out a sync pulse to the slave US system at every image frame and collects an image frame from the slave US system such that both the master and slave systems collect the dual image frames synchronously. The dual system has a scanning frame rate of 64 frames per second. Binary radio frequency (RF) data output is streamed to a solid-state hard drive at the dual ultrasound scanning frame rate. To provide synchronized video output, compact external frame grabbers

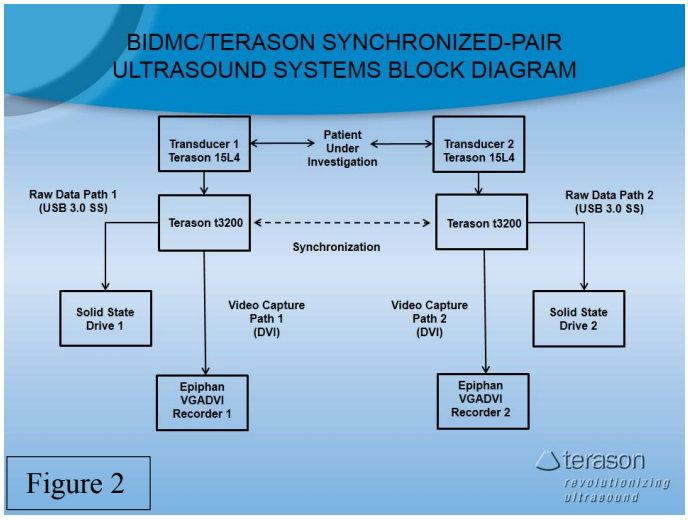

Figure 2

capture the video output (DVI format, 30 frames per second) from each of the Terason T3200 US systems to archive the data in lossless compression format.

Software Development: Workflow to process the stereophotogrammetric images and calculate the 3D vertebral body motion and IVD deformation is outlined in Figure 3. The user specifies a region of interest (ROI) corresponding to the bony profiles of the vertebral body that is then applied to each subsequent image frame. The overall motion of the centroid of that bone profile is calculated by averaging the displacement of all the pixels contained within that bony profile. After the RF stream is recorded on the SSD, a custom C-based software program converts the RF stream to RF data frame sequences. We developed a motion tracking program based on "A Parallelizable Real-time Motion Tracking Algorithm with Applications to Ultrasonic Strain Imaging" (J Jiang, TJ Hall, Phys. Med. Biol. 2007) to compare two consecutive US images and map the lateral (perpendicular to US beam) and axial (parallel to US beam) displacement of pixels comprising the bony profiles of the vertebrae using a block matching algorithm. To discretize the data, kernels corresponding to a width (lateral) and length (axial) of 0.90 and 1.20 mm, respectively, are moved over the RF signal from sequential image frames with 33% axial and lateral overlap. A quadratic fit to the cross-correlation function is used to detect sub-sample motion.

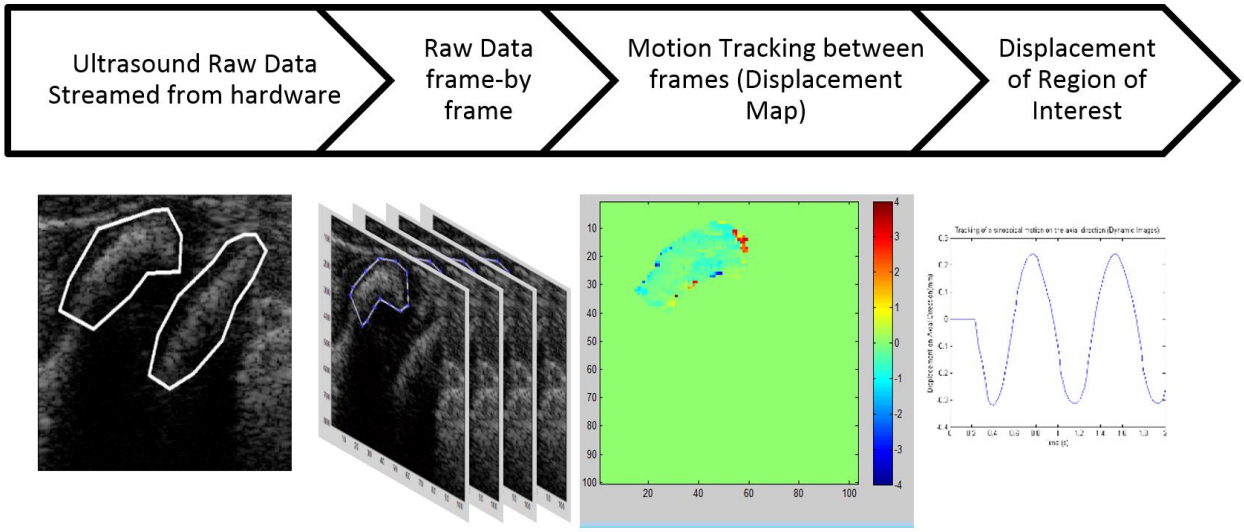

Figure. 3 *Workflow for processing dual US images and calculation of vertebral displacement from sequential images:* A user specified reigion of interest corresponding to the bony profile of the cervical vertebrae (spinous processes of contiguous cervical vertebrae C5 and C6 illustrated) is then tracked on sequential images. The average of the displacements of each pixel contained within that profile is calculated for each sequential image and the overall displacement of the centroid of the bone profile (corresponding to the spinous process of C5) over time plotted.

Task 2*: *Validate dual US system ex-vivo using human cadaver cervical spines mounted in multi-axial servo hydraulic testing machine subjected to physiologically relevant forces and moments

A. Compare deformation of IVD measured using dual ultrasound system to direct measurements

Two 15L4 ultrasound probes (linear transducer, Terason, MA), oriented at a known fixed angle to one another, were synchronized to acquire B-mode ultrasound images of the anterior and posterior profiles of a dynamically loaded *ex-vivo* human C6-7 FSU excised from a 56 years old male (Figures 4 and 5).

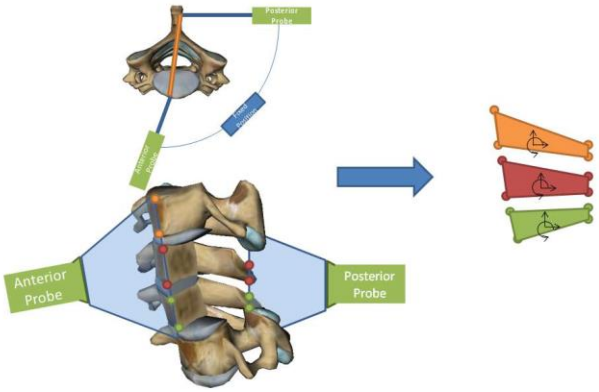

Figure 4 *Stereographic US imaging of cervical spine and simplified rigid body representation of C4-C7*

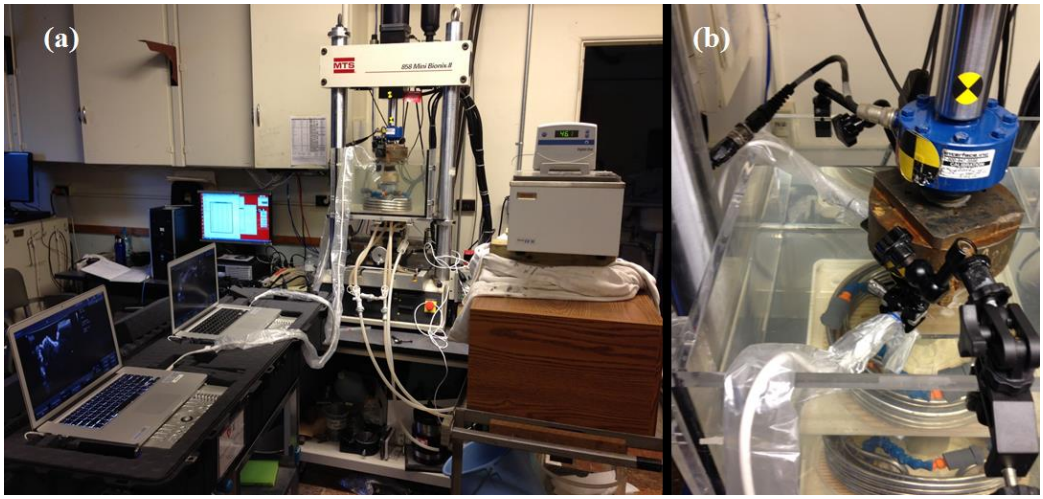

Figure 5 *Human cadaveric C6-7 FSU mounted in MTS servohydraulic load frame immersed in saline bath and imaged using dual ultrasound system in real time. (a) Entire experimental set-up; (b) orientation of ultrasound probes relative to specimen.*

Adjacent vertebral bodies of the C6-7 FSU were rigidly mounted in an MTS material testing system (MTS System Corporation, MA). The entire specimen was submerged in 0.9% saline bath at 37 °C to replicate physiological conditions. The anterior US probe was oriented to image the anterior margins of the vertebral bodies and IVD; the posterior US probe was oriented to image the margins of the spinous processes (Figure 5b). The FSU was subjected to dynamic compressive and distractive loads (-90N to +90N @1-8 Hz. After the user specifies the ROI corresponding to the profiles of the vertebral body and spinous process on the initial image frame, the code is fully automated to calculate the displacement of these anatomic structures over time. The processing time for the RF data-based algorithm is 5 minutes for each 10 second sequence of U/S image frames, compared to 30 minutes using the video-based algorithm. The calculated displacements are highly reproducible and manual correction between consecutive US frames is not needed for the RF-based analysis.

The real time, IVD deformation deduced from the stereographic US images were compared to IVD deformations measured directly using the in-line LVDT of the MTS system. Overall there was good correspondence between the IVD deformations measured using either anterior or posterior anatomic landmarks (Figure 6) compared to IVD

deformation measured directly by the LVDT. The asymmetric deformation of the IVD in compression vs. distraction implies that the IVD is stiffer in compression than tension.

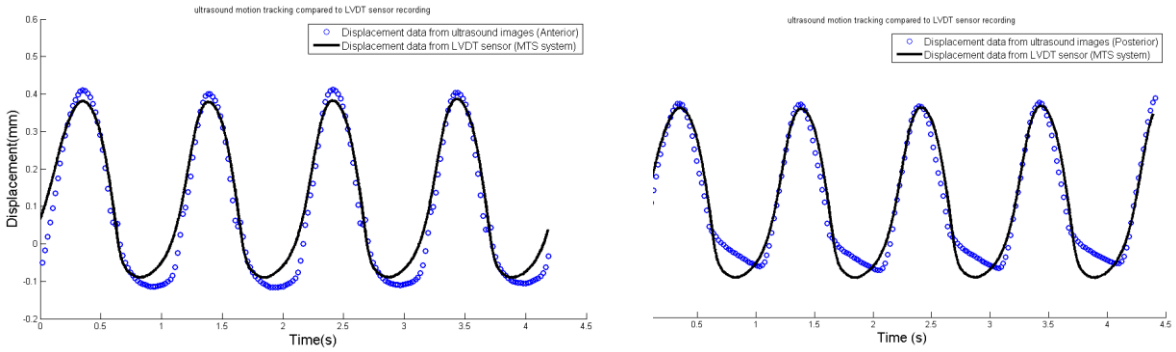

Figure 6 *Representative C6-7 IVD displacement data for FSU subjected to sinusoidal compressive and distractive force -90N to + 90N @ 1Hz. Black curve shows IVD displacement measured by LVDT and blue circles correspond to IVD displacement deduced from the anteriorly positioned probe(left) and posteriorly positioned US probe (right)*

C6-7 IVD deformation deduced by ultrasound using the RF algorithm were highly correlated with IVD deformation measured directly by the LVDT (Table 1; Figure 7). Compared to the video-based tracking algorithm implemented previously (Table 1 and Figure 8), the performance of RF based tracking algorithm demonstrated improved performance for applied frequencies >4Hz: US measures of IVD deformation using the RF algorithm accounted for ~92% of the variation in the IVD deformation measured directly for frequencies up to 6Hz and 77% of the variability in deformation at 8Hz (R^2 =0.77), a significant improvement over the video-based tracking algorithm, R^2= 0.30.

Goodness-of-fit(R^2)

Frequency (Hz)	Raw data-based	Video-based
1	0.95	0.97
2	0.96	0.92
4	0.85	0.80
6	0.91	0.56
8	0.77	0.30

Table 1 *Goodness of fit (Coefficient of Determination, R^2) for IVD deformation deduced by US (RF and Video based) compared to direct measurement*

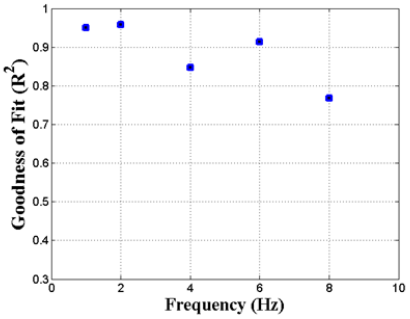

Figure 7 *Coefficients of determination for US vs. LVDT measurement of IVD deformation plotted as function of applied frequency*

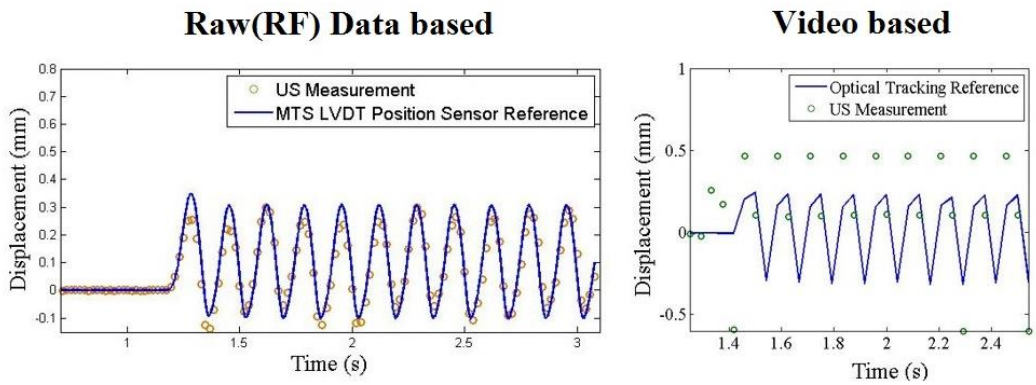

Figure 8 *Representative C6–7 IVD deformation deduced by US using RF algorithm and Video based algorithm compared to deformation measured directly by in-line LVDT for applied -90N to +90N sinusoidal force @ 6Hz. Blue line is LVDT displacement measurement and red circles are displacements deduced from US images. The RF data based motion tracking are highly consistent with LVDT measurements at 6Hz.*

Compared to the video-based motion tracking algorithm used in our previous work, the RF based processing algorithm has better performance with respect to image processing time,

reproducibility and accuracy, especially at higher frequencies (i.e. 6-8 Hz). Based on data from USAARL, the cervical spine of warriors driving in an armored vehicle is exposed to vibrations at frequencies approximating 5-6Hz and up to 8 Hz in a helicopter. Therefore, to be able to analyze the dynamic motion of the C-spine of warriors participating in military operations, the scan rate of the system was optimized to 64Hz (64 frames per second). The improvements to our hardware and software now allow us to track cervical spine motion at frequencies up to 8Hz with >75% confidence.

B. 3D Kinematics using Dual Ultrasound Stereographic Imaging of C-spine Preliminary Studies

We evaluated the ability of the dual ultrasound stereographic imaging system to derive 3D kinematics of a C-spine FSU by applying a pure 1N·m flexion moment to the C6-7 FSU. Ultrasound images of the displacement of the superior + inferior facets and spinous processes were obtained (Figure 9), and used to calculate the Euler angle between contiguous vertebrae, each represented by a plane triangular rigid body (Figures 10 & 11). The calculated instantaneous center of rotation was at the middle column of the vertebra so that in flexion, the anterior IVD compressed, and posterior IVD distracted. The IVD was stiffer in compression than tension.

Figure 9. *The lower vertebral body of the FSU was mounted in PMMA and attached to a plate fixed on a tripod. Four hydraulic pistons were rigidly attached to the PMMA to allow the application of force couples that induced pure flexion-extension or lateral bending moments to the FSU. The dual ultrasound probes were oriented to image the facet joints and spinuous processes of C6-7.*

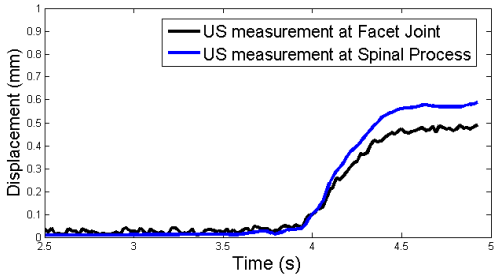

Figure 10 *Displacement measured at facets and spinous processes by US during applied flexion moment*

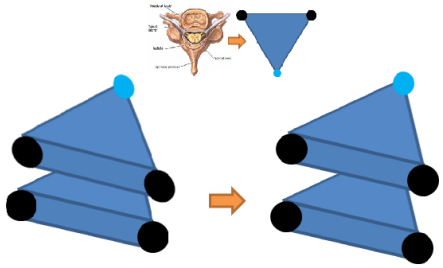

Figure 11 *Rigid body motion of FSU represented by triangular shaped vertebrae. Animated model using stereographic ultrasound images to generate Euler angles.*

<u>Task 3:</u> Examine relationship between "health" of IVD measured on static MRI images vs. mechanical compliance of FSU measured by US

The feasibility of using US to measure the functional performance of cervical spine FSUs was evaluated by plotting the static and dynamic deformation of the IVD measured by US as a function of the applied load. A single US probe was oriented in the anterior "window" between the sternocleidomastoid muscle and carotid artery of human cadaveric cervical spine specimens obtained from elderly individuals (age 73-91). The C4-5 and C5-6 FSUs were evaluated as these levels are most commonly affected by degenerative disc disease, presumptively as a consequence of chronic overloading. Consistent, standardized anatomic landmarks corresponding to the intersection of the anterior vertebral body cortical shell with the vertebral body endplate adjacent to the IVD were identified and this profile tracked on all subsequent US images of the FSU.

Age	VD level	Static Compliance (mm/N)	Dynamic Compliance (mm/N)	Area Estimate (N·mm)	Pfirrmann grading
91	C4-5	3.37E-03	3.68E-03	9.08	4
	C5-6	2.25E-03	2.00E-03	9.98	4
81	C4-5	2.25E-03	2.28E-03	18.48	4
	C5-6	7.42E-03	1.10E-02	18.78	4
81	C4-5	5.62E-03	1.09E-02	29.36	4
	C5-6	6.29E-03	8.06E-03	28.7	5
73	C4-5	6.74E-04	1.51E-03	91.84	5
	C5-6	1.12E-03	1.72E-03	62.05	5

Table 2. *Compliance and damping coefficient derived for C4-5 and C5-6 FSU levels from each specimen*

Static and dynamic compliances measured directly and by US are summarized in Table 2. The static compliance of the FSU was calculated as the slope of the deformation of the IVD in response to statically applied compressive and distractive forces of 20 lbs. to C4-C5 and C5-C6 (Figure 12). A simplified linear approximation of the dynamic compliance was calculated using linear regression to the non-linear data set to evaluate and compare the static compliance to the dynamic compliance (Figure 13). Damping, which represents the lost work during each load cycle, was calculated from the area between the loading and unloading trajectories of the force-displacement curve. There was significant variation among the specimens, but the mean compliance for the C4-C5 FSU measured statically and dynamically

by US was 2.98×10^{-3} mm/N, 4.59×10^{-3} mm/N respectively and the mean compliance for the C5-C6 FSU measured statically and dynamically by US was 4.27×10^{-3}, 5.70×10^{-3} mm/N respectively. For this small number of specimens (lack of power), we could not demonstrate significant differences (1-way ANOVA) between the static or dynamic compliance of C4-C5 and C5-C6, nor demonstrate an effect of age. Considering the elderly ages of these specimens, this finding is not inconsistent with our previous finding that C4-C5 is more compliant than C5-C6 in younger aged specimens. The static compliance measured by applying a 20 lb. compressive and distractive load was positively correlated the with dynamic compliance measured directly (R = 0.6) and by US (R = 0.9) for a dynamic displacement of 1mm at 1Hz, suggesting that this static test, while ignoring the viscoelastic behavior of the IVD might be a useful clinical test performed in the office to predict the overall dynamic mechanical behavior of the FSU.

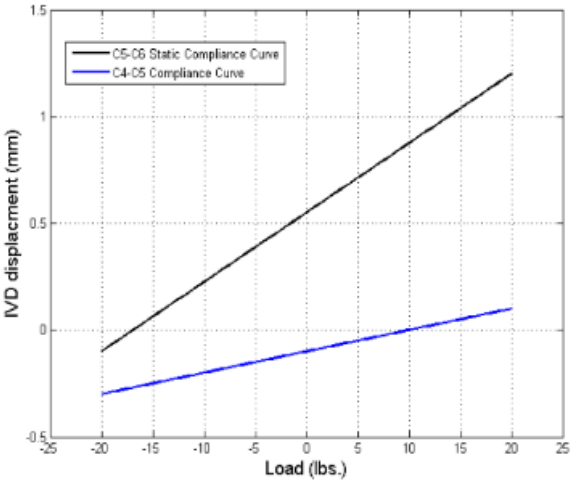

Figure 12 *Representative static displacement-load curves for C4-C5 and C5-C6 FSUs to calculate static compliance (slope)*

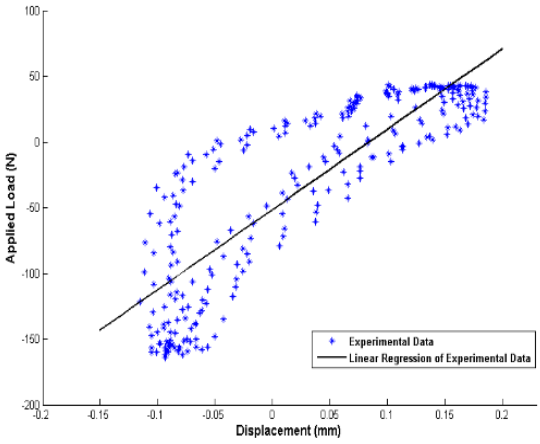

Figure 13 *Representative dynamic load – displacement data for C4-C5 and C5-C6 FSUs. Line fit to the non-linear data to derive linear (elastic) estimate of dynamic compliance*

The integrity of cadaveric C-spine IVD was also evaluated from MRI T2-images using Pfirrmann scale. Not unexpectedly, because of the advanced ages of the specimens, most of the IVDs were degenerated: grade 4 or 5. For this limited number of specimens, the linear (elastic) approximation of the static and dynamic compliance of the C4-5 and C5-6 FSUs were affected by the integrity of the IVD as measured by Pfirrmann grade (1-Way ANOVA, $p<0.05$). The damping coefficient was unaffected by the Pfirrmann grade. This finding is consistent with the observation that the "health" and integrity of the IVD affects the mechanical performance of the FSU and that our US system may provide a cost-effective clinical tool to evaluate the integrity and performance of the IVD by applying low amplitude traction and compressive loads to the head and neck *in-vivo*.

Recognizing the deficiencies of modeling the dynamic mechanical properties of the cervical spine FSU using a linear approximation, we collaborated with our subcontractor at Medical College of Wisconsin to generate more sophisticated non-linear models that better fit the dynamic force-displacement data and account for the differential elastic and viscoelastic response during cyclic loading in tension and compression (Figure 14). Focusing on the C4-5 FSU, this differential mechanical behavior is evident as the specimen is initially loaded to 50 N in tension (A-B), followed by tensile unloading (B-C), then compressive loading to 150 N (C-D)

followed by unloading and "recoil" (D-A). The unloading path did not follow the loading path, consistent with Mullin's effect. Also, the IVD strain "softened" in tension and compression as the peak strain increased with progressive loading cycles. The stiffness during tensile and compressive loading was approximately 300 and 800 kN/m.

The force-displacement data was converted to stress-strain data based on the following equations:

$$Stress = \frac{Force}{Area} \qquad (1)$$

$$Strain = \frac{Change\_In\_Length}{Original\_Length} \qquad (2)$$

The average cross-sectional area of C4-5 disc was assumed to be 400 mm^2 (Pooni, Hukins et al. 1986) and the average disc height was assumed to be 3.3 mm (Pait, Killefer et al. 1996). The corresponding stress-strain response is shown in Figure 15.

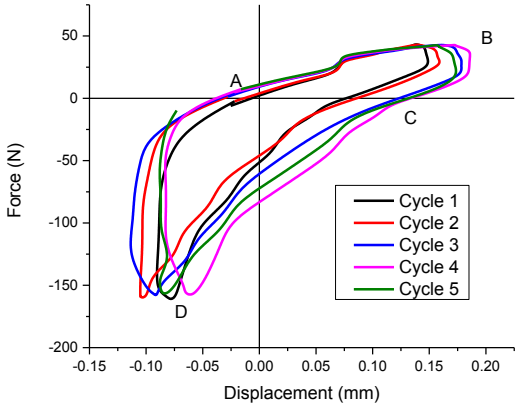

Figure 14 *Force-Displacement data for C4-5 segment*

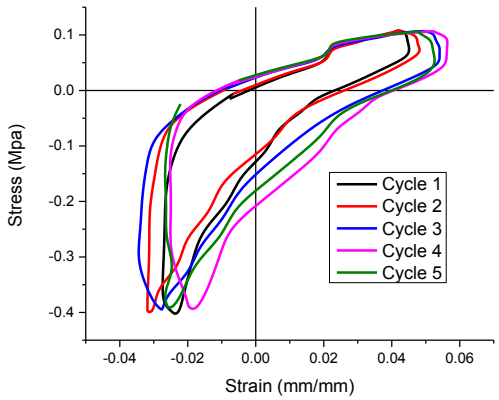

Figure 15 *Sterss-Strain data for C4-5 segment*

The next phase in the analysis was to arrive at an appropriate nonlinear mathematical function (material model) representing the observed stress-strain responses. For this purpose, the coefficients in the nonlinear function were optimized using a generic algorithm C++ toolbox (Sastry and Goldberg 2007). The optimization scheme involved the evaluation of the "fitness of error," defined as the difference between the experimental response and the model response in one cycle over the entire loading-unloading sequence. The "fitness of error" is given in Equation(3). The lower the fitness, the better the agreement between the experimental data and analytical model. Six nonlinear material models (finite element) were identified and calibrated to minimize the error. The model that best correlated with the experimental data was used.

$$Fitness,\ f(X_1, X_2 \ldots X_n) = \sqrt{\frac{\sum_i^n \left(F_i^{\exp} - F_i^{eval}\right)^2}{n}} \qquad (3)$$

Where: X_i = Variables to optimize; n = Number of data points

$F_i^{\exp}$ = Experiment data; F_i^{eval} = Evaluated model data

This "Three Network Model" represented the differential material properties of the FSU/IVD complex. In the model, the IVD material is represented using three distinct structural domains that capture the experimentally observed non-linear, time- (and expected temperature)-dependent response at both small and large strains. The governing constitutive equation for the Three Network Model is given in Equations (4)-(6). The optimized fit to the experimental data after convergence is presented in Figure 16. The final converged "fitness of error" was 9.8 N. The goodness-of-fit, r-squared value, associated with this was 0.98.

$$\sigma_A = \frac{\mu_A}{J_A^e \lambda_A^e} \frac{L^{-1}(\lambda_A^e / \lambda_L)}{L^{-1}(1/\lambda_L)} dev[b_A^e] + \kappa(J_A^e - 1) \tag{4}$$

$$\sigma_B = \frac{\mu_B}{J_B^e \lambda_B^e} \frac{L^{-1}(\lambda_B^e / \lambda_L)}{L^{-1}(1/\lambda_L)} dev[b_B^e] + \kappa(J_B^e - 1) \tag{5}$$

$$\sigma_C = \frac{1}{1+q} \left\{ \frac{\mu_C}{J\lambda_C^e} \frac{L^{-1}(\lambda_C^e / \lambda_L)}{L^{-1}(1/\lambda_L)} dev[b_C^e] + \kappa(J_C^e - 1) + \mathrm{q} \frac{\mu_C}{J_C^e} \left[I_1 b_C^e - \frac{2I_2}{3} I - (b_C^e)^2 \right] \right\} \tag{6}$$

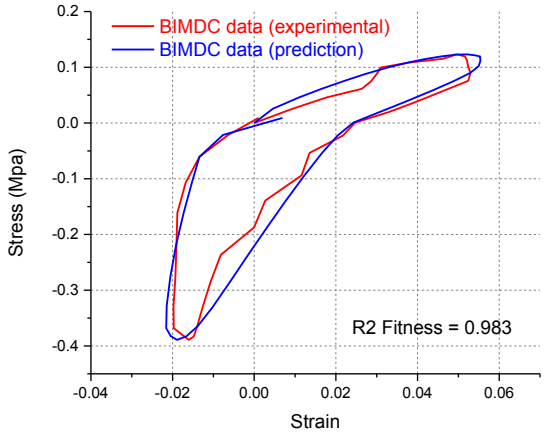

Figure 16 *Final optimized fit*

<u>Task 4</u>: Develop custom cervical collar to maintain dual ultrasound probes in proper alignment for imaging anterior and posterior C-spine anatomic landmarks in-vivo.

A cervical collar, comprised of a modified motocross EVS RS-Evolution (Rancho Dominguez, CA) race collar was developed (Figure 17). The collar holds the dual Terason 15L4V US probes against the subject's neck in the proper orientation to acquire posterior and anterior image projections of the C-spine *in-vivo*. Two articulating arms (Ultraflexx) allow the contact force against the subject's neck to be adjusted so as to obtain consistent US images. A Tethertools mini-clamp locks each US probe in its final position. The probes and cervical collar did not inhibit neck motions (rotation, flexion and extension) with and without the subject wearing a standard issue Army helmet (Figure 18).

Figure 17*: Custom cervical collar for maintaining position of dual US probes. Top: anterior probe; bottom: posterior probe held by clamps*

Figure 18 *Dual Ultrasound System with subject wearing Army Helmet*

Acquired dual ultrasound images of anterior vertebral body and posterior spinous process at C4 and C5 levels are shown in Figure 19.

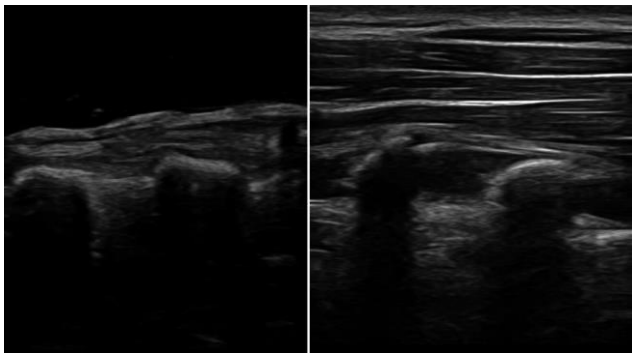

Figure 19 *B-mode Ultrasound Image acquire from anterior (left, anterior vertebrae body imaged) and posterior (right, spinal processes imaged)*

<u>Task 5.</u> Use US to measure C-spine motion and IVD deformation in-vivo in human volunteers to evaluate the static and dynamic mechanical properties of the C-spine during simulated operational conditions with and without headgear

In order to derive a transfer function for the mechanical behavior of the cervical spine *in-vivo* in a consistent and reproducible way, a system similar to standard cervical spine traction used by physical therapists to treat neck pain is being developed that can apply cyclic loads to the head and neck over a range of frequencies up to 8 Hz. This system will allow us to conduct a parametric analysis of the effect of varying load amplitudes and frequencies on the elastic and damping coefficients of individual FSU's *in-vivo*. The system is composed of a weighted helmet and a solenoid based load actuator driven by a programmable DC power supply that applies a variable traction force to the weighted helmet via a pulley/cable system (Figure 20). Load transducers mounted in the helmet (in contact with the head) and a force plate on the ground measures the force applied to the head/neck and torso of the subject while sitting or standing.

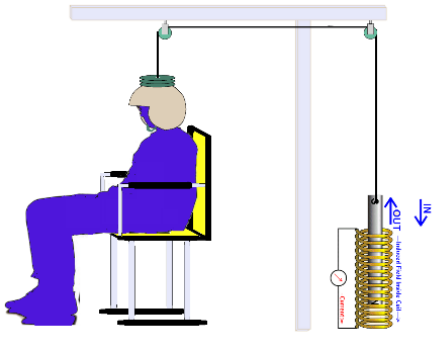

Figure 20 *Schematic of cyclic load application system to head/neck of subject while sitting or standing in load frame.*

The design concept was tested using cadaveric cervical spine specimens (Figure 21) and compared to data generated using a servo-hydraulic test system (Instron 8811, Norwood,

MA). The applied force was measured with load cell in series with the spine. A 1Hz frequency square wave with load amplitude of 20 lbs was applied to the entire cadaveric cervical spine, C1-T1, while the deformation at the C4-5 and C5-6 FSUs were measured in real time using an optical tracking system and the US probes. The resultant load - displacement curves for the cadaveric C-spine were similar for the solenoid-based traction system and the Instron servohydraulic system (Figure 22), however the solenoid-based transducer was unable to dampen the initial impulse of the applied weight to the spine (evidenced by transient spikes at initial application of force).

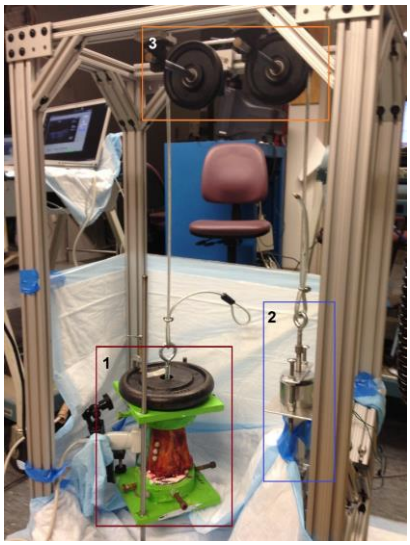

***Figure* 21** *The prototype system is composed of a load frame to which the spine specimen is mounted. A fixed weight* [Box 1] *was rigidly mounted to the atlas (C1) to provide a constant compressive force to the entire C-spine. A solenoid-based load actuator* [Box 2] *(Magnetic Sensor Systems, Van Nuys, CA) driven by programmable DC power supply (Genesys, TDK-Lambda, NJ) applies a variable traction force to the fixed weight via pulley/cable system* [Box 3] *so that a known, variable, cyclic load can be applied to the spine while the resulting displacement of the FSUs are measured by US and the optical tracking system (reflected markers shown on spine* [Box 1].

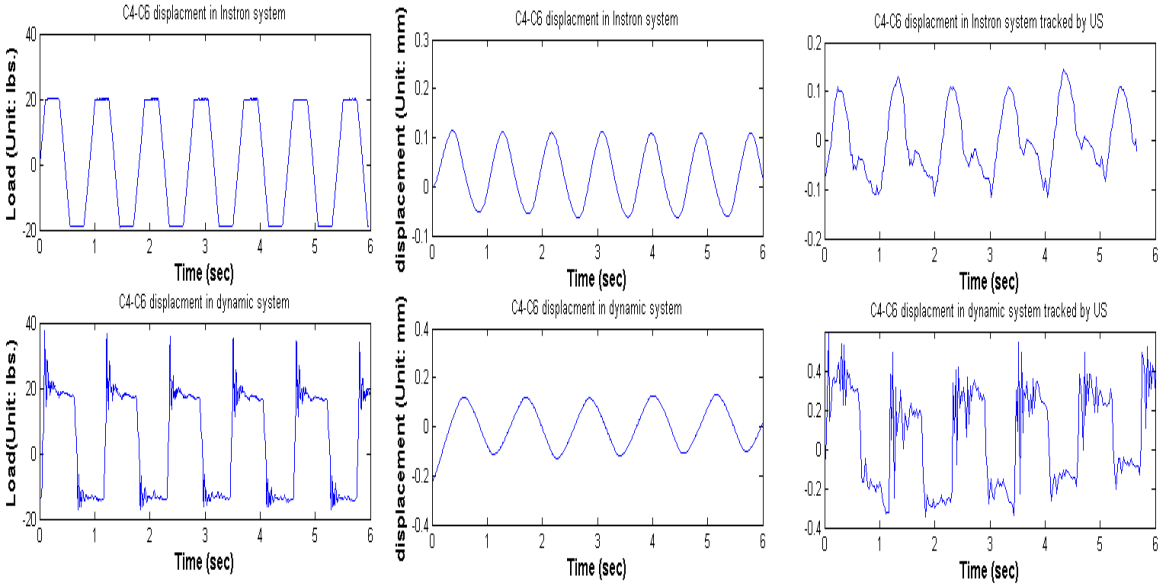

Figure 22 *Comparison of load and displacement measured directly and by US for C4-C6 using Instron vs. solenoid based traction system for cadaver specimens.*

The deformation between C4 and C6 measured by the US probe was affected by bulging of the IVD and soft tissues during compressive loading as evidenced by the dicrotic wave form observed consistently during compression at the “valley” of the cyclic displacement curve for both the servo-hydraulic and solenoid-based load actuators. However, the deformation of C4-6 measured by the US probe in distraction was also affected by high frequency vibrations

induced by the traction impulse applied to the spine by the solenoid actuator (Figure 22).

We also tested the solenoid based traction system on ourselves. A 10 lb. load was applied to the neck, cyclically alternating between distraction and compression (Figure 23). To ensure that the central axis of the head and neck were collinear with the applied uniaxial force, a 5 point latch & link restraint system was used to fix the torso of the sitting subject in the load frame along the line of action of the cable. So that load is safely applied to the neck, the subject wears a well-padded, tight fitting helmet with an attached 10 lb. weight that applies a constant compressive load to the spine which is then "unloaded" by the application of an increasing traction force generated by the solenoid-based load actuator via a cable attached to the weight. A load cell interposed between the weight and the helmet measures the resultant force applied to the neck in real time (iLoad Mini, Loadstarsensor, Fremont, CA). For this preliminary trial, a square-wave function was used to apply a 0 to 20lb traction force via the solenoid to cyclically load the neck between -10 to +10 lbs. The dual US system was used to measure the resulting dynamic motion of the C4-5 and C5-6 FSU's. The anterior US probe imaged the anterior profile of the C4-5-6 vertebral bodies and interposed discs; the posterior US probe imaged the profiles of the corresponding spinous processes.

Preliminary test data is shown in Figure 24. Similar to the cadaver test, the initial impulse applied to the head/neck by the traction load generated by the solenoid actuator created undesirable high frequency vibrations at the initiation of the applied step loads. These transmitted vibrations were reflected in the measured C4-C5 displacements. These high frequency vibrations will be addressed by interposing a spring to dampen the initial load impulse. Alternatively, a pneumatic powered load actuator might allow more controlled load application than the solenoid based actuator.

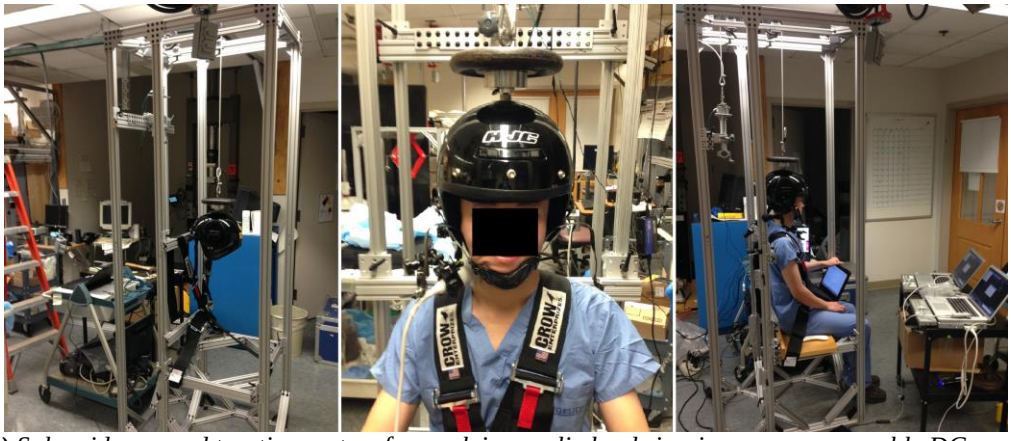

Figure 23 (a) *Solenoid powered traction system for applying cyclic loads in-vivo: a programmable DC power supply is used to power a solenoid that applies a variable traction force via two fixed pulleys to a fixed weight attached to the top of the helmet;* ***(b)*** *front view* ***(c)*** *and side view demonstrating restraints and dual ultrasound probes positioned on the subjects neck anteriorly and posteriorly in a fixed orientation*.

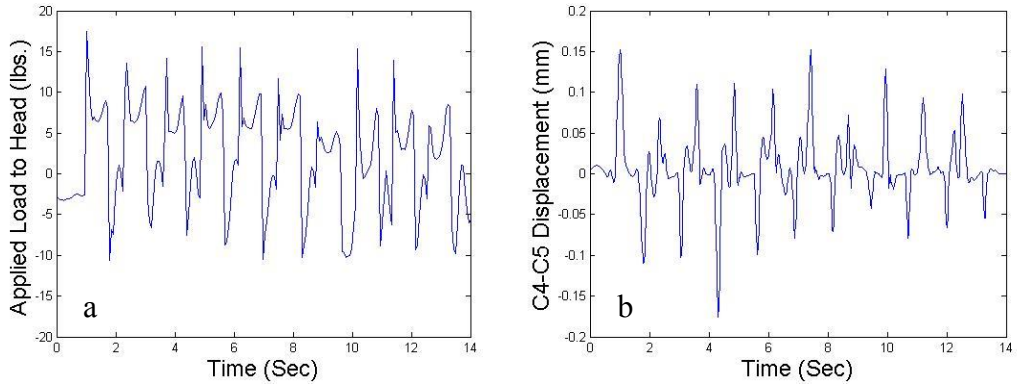

Figure 24 (a) *cyclic tensile/compressive step load applied to head* ***(b)*** *resultant C4-C5 displacement measured by US*

<u>Task 6</u> Develop analytic models from ex-vivo simulations to specify limits on permissible load amplitudes, load rates, # cycles for different loading modes applied to C-spine during operational conditions (Task 11 in Proposal)

A finite element model of C4-C7 developed from CT scans of cadaveric human C-spine has been developed (Figure 25). The osteo-ligamentous material properties assumed for each of the elements were ascertained from the literature. The model was then subjected to pure flexion and extension moments similar to the experiments performed in task 3. The overall rigid body motions of the vertebrae and deformations of the IVD and interposed ligaments were extracted from the displacement map. Predicted responses are were within the mean ± one standard deviation of the experimental data (Figure 26). The resultant motion of the FSU's and deformation of the IVD in flexion and extension are shown (Figure 27). These results suggest that this model can be interfaced with the force-displacement data generated from the *in-vivo* traction-compression loading and FSU displacements measured by the dual US system as part of task 5 to calculate local osteo-ligamentous strains and IVD deformation in response to applied external loads.

Figure 25 *Finite element representations of subaxial cervical vertebra (left, as viewed from top), intervertebral disc (second from left, axial view), facet joints (third from left, sagittal view), loading device (fourth from left) and the sagittal view of the C4-C7 spinal column with the loading device at the superior end (right).*

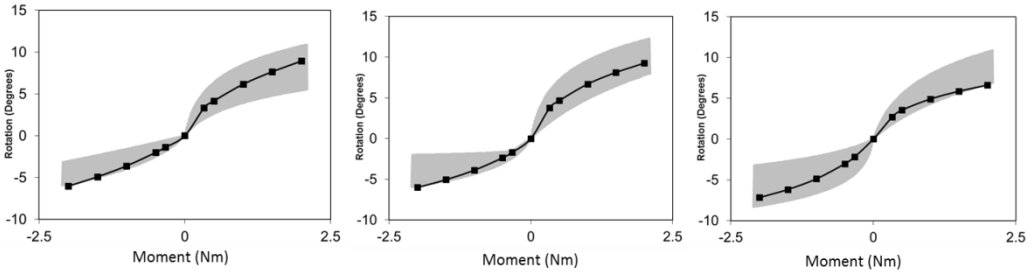

Figure 26 *Moment-rotation kinematics of C4-C5-C6 motion segments subjected to physiological flexion-extension moments*

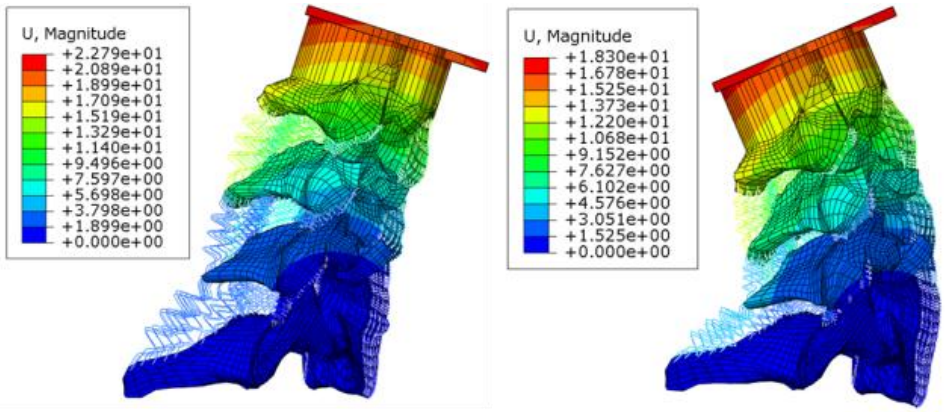

Figure 27 *Displacement map of C4-5-6 motion segments subjected to physiologic flexion (left) and extension (right) moments. Color scale represents the magnitude of deformations represented by the elements.*

The FEM of the cervical spine was updated to be more relevant to the military population. It has improved geometry, uses a finer mesh, has an increased number of elements and includes an additional spine segment. These refinements will improve the capability of the FEM to simulate different types of loadings and expand the model's responsiveness making it more suitable to carry out parametric studies.

The geometry of the cervical spine FEM was updated using data from the Global Human Body Model Consortium. In the previous FEM, the nodes at the inferior margin of the C7 vertebrae were constrained. The T1 vertebra was added to the updated model to better represent the foundation of the cervical spine. The updated model (C4-T1) is based on anthropometric specifications for a mid-size male (175 lbs.), in contrast to the previous generic model generated from a female cadaver. Since this model was developed for use in LS-DYNA software, it needed conversion to the ABAQUS solver to perform stress analysis. As the two finite element software packages have different built-in material models and element types, the conversion tasks included: input deck compatibility, element type compatibility, and material model compatibility. The previous FEM consisting of 18731 mesh elements and 24086 nodes was improved to have a finer mesh consisting of 65316 elements and 48302 nodes (Figure 28). The finely meshed IVDs at C4-5, C5-6, C6-7 and C7-T1 better mimic the actual geometry (Figure 29). Tie constraints between the bony endplates of the vertebrae and cartilaginous endplate of the discs were added to all segments.

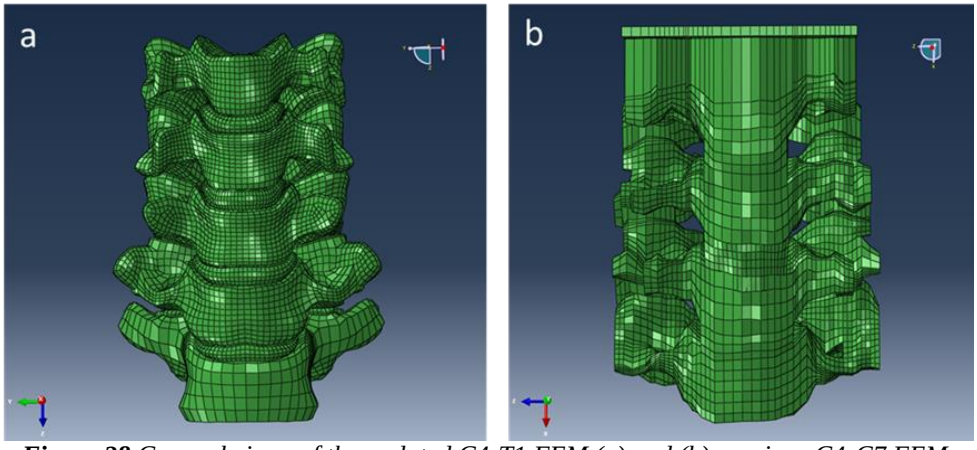

Figure 28 *Coronal views of the updated C4-T1 FEM (a) and (b) previous C4-C7 FEM*

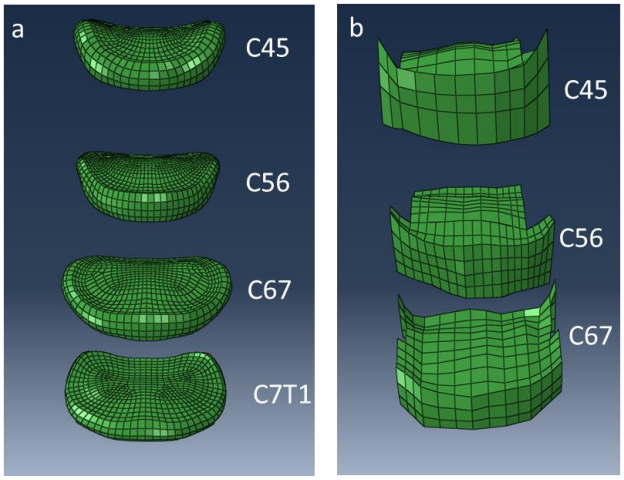

Figure 29 *Geometry of IVD (a) updated C4-T1 FEM and (b) previous C4-C7 FEM*

In addition elements corresponding the ligaments and soft tissue connections that provide stability to the cervical spine FSUs were added (Figures 30 and 31). For the anterior longitudinal ligament, a total of 324 connector elements were used between C4 to C7 (12 elements wide and 27 elements long). Elements representing the interspinous ligaments, facet joint capsule and ligamentum flavum are now included in the updated FEM.

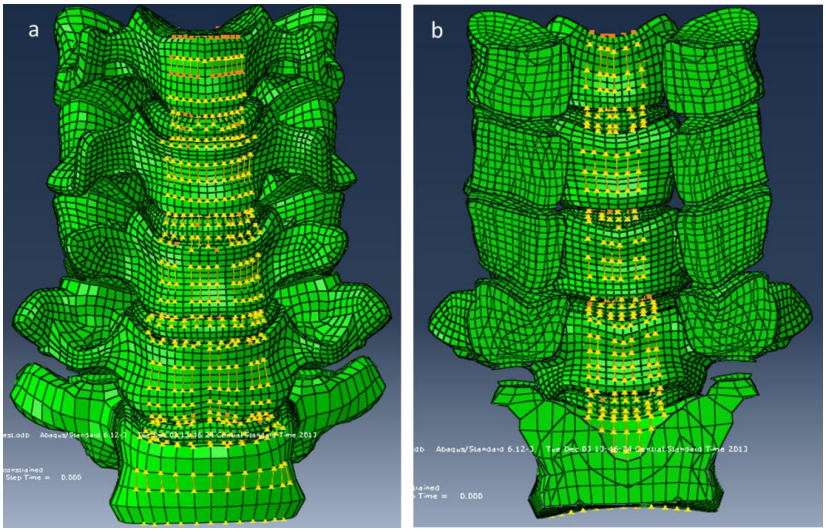

Figure 30 *Ligaments attachment to the updated model: (a) anterior longitudinal ligament, and (b) posterior longitudinal ligament shown by sectioning c-spine in coronal plane*

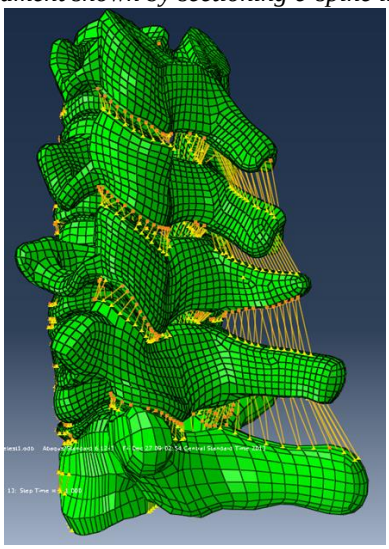

Figure 29 *Updated model showing the facet joint capsule, interspinous ligament and ligamentum flavum*

A rectangular plate was attached to the superior endplate of the C4 vertebrae using mesh manipulation software (ANSA). The plate helps in the application of pure moments by applying a force couple along anterior and posterior edges of the plate. The plate can be also be used to simulate other experimental load scenarios and the mass imposed by a helmet.

During the next quarter the finite element analysis will proceed as follows:

1. Subject the updated model to experimental *ex-vivo* and *in-vivo* load conditions .
2. Extract internal parameters such as stresses, strains and strain energy densities in various regions of the disc from the abacus solver, from stress analysis outputs.

3. Use outputs extracted in step two and include experimental output conditions: incorporate the US-measured deformation/strain fields over the fatigue period, simulating cyclic loading conditions, to a fatigue solver.
4. From the fatigue solver, determine the 'life span' of the spine for the inputted experimental condition, described in step one.
5. Exercise the finite element stress analysis and fatigue solver models to different parametric conditions such as the effect of added mass and locations that may be off-center from the center of gravity/mass of the neck to predict the 'life span' under these conditions.

Reportable Outcomes

PUBLICATION

Dynamic Ultrasound Imaging of Cervical Spine Intervertebral Discs, 2013 IEEE Ultrasonics Symposium Proceedings
Clinical Ultrasound Can Measure Static and Dynamic Cervical Spine Intervertebral Disc Properties, Radiology (submitted)
Sensitivity and Stability Analysis of a Nonlinear Material Model of Cervical Intervertebral Disc Under Cyclic Loads Using the Finite Element Model, Rocky Mountain Bioengineering Symposium 2014(submitted)
Real Time Ultrasound Can Measure Dynamic Properties of Cervical Spine Intervertebral Disc, ORS 2014 Annual Meeting (accepted as poster)
3D Kinematics Using Dual Ultrasound Stereographic Imaging of Human Cervical Spine, 85th Annual Scientific Meeting of the Aerospace Medical Association (accepted as slide presentation)
Dynamic Ultrasound Imaging of Cervical Spine Intervertebral Discs, World Conference of Biomechanics 2014 (submitted)
Role of Nucleus Pressure in the Cyclic Response of Intervertebral Disc, World Conference of Biomechanics 2014 (submitted)

Conclusion

We developed a unique dual ultrasound system that can non-invasively measure IVD deformation and mechanical compliance *ex-vivo*, and provide real-time images of IVDs and dynamic vertebral motion *in-vivo* during simulated tasks relevant to acute and chronic cervical spine injury and disease. A semi-automated program was developed to track the motion of a user-specified region of interest that corresponds to the anterior and posterior bony profiles of cervical vertebrae. Dynamic IVD displacements of vertebrae C4-5 measured by US were consistent with direct measurements. For motion frequencies up to 8Hz, US accounted for 77-96% of the true IVD displacements. We developed a transfer function that modeled the non-linear displacement of human cadaveric cervical spine functional spine units (FSU) as a function of an applied sinusoidal load that accounts for differential compliance and damping coefficients in tension and compression. A FEM of the cervical spine was updated to be more relevant to the military population. It has improved geometry, uses a finer mesh, has an increased number of elements and includes an additional spine segment. These refinements will improve the capability of the FEM to simulate different types of loadings and expand the model's responsiveness making it more suitable to carry out parametric studies. We developed a diagnostic system that applies

dynamic cyclic loads to cervical spine over a range of programmable frequencies and amplitudes that simulate operational conditions.

References

Pooni, J. S., et al. "Comparison of the structure of human intervertebral discs in the cervical, thoracic and lumbar regions of the spine." Surgical and radiologic anatomy 8.3 (1986): 175-182.

Pait, T. Glenn, James A. Killefer, and Kenan I. Arnautovic. "Surgical anatomy of the anterior cervical spine: the disc space, vertebral artery, and associated bony structures." Neurosurgery 39.4 (1996): 769-776.

Sastry, Kumara, David E. Goldberg, and Xavier Llora. "Towards billion-bit optimization via a parallel estimation of distribution algorithm." Proceedings of the 9th annual conference on Genetic and evolutionary computation. ACM, 2007.